JBC Papers in Press. Published on April 26, 2016 as Manuscript M115.708347
The latest version is at http://www.jbc.org/cgi/doi/10.1074/jbc.M115.708347

Contribution of Tyr^{B26} to the Function and Stability of Insulin

STRUCTURE-ACTIVITY RELATIONSHIPS AT A CONSERVED HORMONE-RECEPTOR INTERFACE

Vijay Pandyarajan[1], Nelson B. Phillips[1], Nischay Rege[1], Michael C. Lawrence[2,3], Jonathan Whittaker[1], & Michael A. Weiss[1,4,5*]

[1]From the Departments of [1]Biochemistry, [4]Medicine and [5]Biomedical Engineering, Case Western Reserve University, Cleveland, OH 44106 USA
[2]The Walter and Eliza Hall Institute of Medical Research, 1G Royal Parade, Parkville, Victoria 3052, AUSTRALIA
[3]Department of Medical Biology, University of Melbourne, Parkville, Victoria 3010, AUSTRALIA

*Running title: *A Conserved Tyrosine at a Hormone-Receptor Interface*

To whom correspondence should be addressed: Michael A. Weiss, Departments of Biochemistry, Medicine and Biomedical Engineering, Case Western Reserve University, Cleveland, OH 44016 USA; Tel.:+1 216 368 5991;E-mail: michael.weiss@case.edu

Keywords: hormone, diabetes mellitus, receptor tyrosine kinase, non-standard mutagenesis, protein structure

ABSTRACT

Crystallographic studies of insulin bound to receptor domains have defined the primary hormone-receptor interface. We investigated the role of Tyr^{B26}, a conserved aromatic residue at this interface. To probe the evolutionary basis for such conservation, we constructed 18 variants at B26. Surprisingly, non-aromatic polar or charged side chains (such as Glu, Ser, or ornithine; Orn) conferred high activity whereas the weakest-binding analogs contained Val, Ile and Leu substitutions. Modeling of variant complexes suggested that the B26 side chains pack within a shallow depression at the solvent-exposed periphery of the interface. This interface would disfavor large aliphatic side chains. The analogs with highest activity exhibited reduced thermodynamic stability, and heightened susceptibility to fibrillation. Perturbed self-assembly was also demonstrated in studies of the charged variants (Orn and Glu); indeed, the Glu^{B26} analog exhibited aberrant aggregation in either the presence or absence of zinc ions. Thus, although Tyr^{B26} is part of insulin's receptor-binding surface, our results suggest that its conservation has been enjoined by the aromatic ring's contributions to native stability and self-assembly. We envisage that such classical structural relationships reflect the implicit threat of toxic misfolding (rather than hormonal function at the receptor level) as a general evolutionary determinant of extant protein sequences.

Insulin, a small globular protein critical to the maintenance of metabolic homeostasis (1), provides a classical model for studies of protein structure and self-assembly (2) with long-standing application to human therapeutics (3). Insulin contains two polypeptide chains, designated A and B, that are linked by two disulfide bridges (cystines A7-B7 and A20-B19); the A chain is further stabilized by an intra-chain bridge (cystine A6-A11). In pancreatic β-cells insulin is stored within glucose-regulated secretory granules as zinc-coordinated hexamers (Fig. 1*A*). The hormone binds to a receptor tyrosine kinase (TK), designated the insulin receptor (IR). The product of a single gene, the IR precursor is processed in the trans-Golgi network into its final disulfide-linked $(\alpha\beta)_2$ homodimer conformation. The extracellular α subunit contains hormone-binding elements whereas the transmembrane β subunit contains the intracellular TK domain (4). Alternative splicing leads to two receptor isoforms, IR-A and IR-B (5). The three-dimensional structure of the holoreceptor has been visualized only at low resolution (>20 Å), but these findings have been inconclusive (for review, see (6)). How extracellular binding of insulin alters the structure of the receptor, leading in turn to activation of the intracellular TK domains is a major unsolved problem (7).

Dissection of the IR into discrete domains has enabled crystallographic analysis of its parts. The relevant structural biology is as follows. (i) Structures of the intracellular TK domains at 1.9 Å resolution have been obtained, and their mode of interaction has been determined (8,9). (ii) The structure of the N-terminal three domains of the α subunit (Leu-rich domain 1, Cys-rich domain and Leu-rich domain 2; L1-CR-L2) has been determined at 2.3 Å (10) and is

similar to the homologous fragment of the Type 1 insulin-like growth factor receptor (IGF-1R) (11). (iii) A lower-resolution structure (3.8 Å) has been determined of the dimeric ectodomain (containing the entire α subunit and the extracellular portion of the β subunit; $(\alpha\beta_\Delta)_2$). This structure (Fig. 1*B*) enabled the orientation of the L1-CR-L2 fragment to be determined relative to fibronectin-III homology domains 1, 2 and 3 (FnIII-1, FnIII-2, FnIII-3). An insert domain (ID) within FnIII-2, including the insulin-binding element (αCT) within the C-terminal region of the α subunit, was incompletely traced in the electron-density map. The overall conformation of the $(\alpha\beta_\Delta)_2$ ectodomain resembles an inverted-V in which the presumed high-affinity site of insulin binding lay within the crux of the dimer (12). An improved crystallographic model of the ectodomain has recently been described (12).

A recent structural advance exploited domain-minimized models of the α subunit containing the primary insulin-binding elements L1 and αCT. Notably, a co-crystal structure has been determined at 3.5 Å resolution of a ternary complex between insulin, an L1-CR fragment and a synthetic αCT peptide spanning residues 704-719 of IR-A (4). In this structure (designated the micro-receptor (μIR) complex) the C-terminal segment of the insulin B chain is detached from the hormone's α-helical core; such detachment is incompatible with classical structures of insulin (Fig. 1*C*) but enables insertion of this segment (including Tyr^{B26}; *red* and asterisk in Fig. 2*A*) between the conserved surfaces of L1 and the αCT peptide (Fig. 2*B*, *C*). This mode of binding, long anticipated based on studies of anomalous insulin analogs (13,14) and residue-specific photo-crosslinking (15), has defined the binding surfaces in the μIR for insulin's conserved triplet of aromatic residues, Phe^{B24}, Phe^{B25} and Tyr^{B26} (Fig. 2*A*). Surprisingly, whereas the side chain of Phe^{B24} inserts within a classical nonpolar pocket (anchoring the displaced B-chain β-strand; (16)), the B25 and B26 side chains appear less closely packed (Fig. 2*B-D*). The latter side chains—despite their broad conservation (17) and the efficient IR photo-crosslinking as photo-activatable derivatives (15,18,19)—appear to contact the μIR surface only loosely.

Our interest in Tyr^{B26} was motivated by its broad conservation among vertebrate insulins (17) and insulin-like growth factors (IGF-I and IGF-II) (20,21). Classical structure-activity relationships at B26 are complex, presumably because of a subtle interplay between *direct* effects of modifications at the hormone-receptor interface and *indirect* effects of conformational changes at this interface. Whereas substitution of Tyr^{B26} by Phe impairs IR affinity by twofold (22)—a finding consistent with a specific (although modest) contribution by the *para*-OH group—studies of an Ala substitution have given rise to conflicting results (23-25). Although apparently dispensable in a truncated yet active insulin analog lacking residues B26-B30 (*des*-pentapeptide[B26-B30]-insulin-amide; DPA (26,27)), mutations or non-standard modifications at B26 in full-length or truncated insulin analogs may impair or enhance activity (28,29). Thus, no coherent pharmacophore has been obtained.

To clarify the contribution of Tyr^{B26} to receptor binding, we undertook a systematic mutational survey based on the semi-synthetic preparation of 18 insulin analogs. In accordance with the peripheral B26-related interface in the μIR complex (4), this survey revealed that high IR affinity can be conferred by non-aromatic polar or charged side chains (either acidic or basic). Although well tolerated at the receptor interface, these substitutions were observed to impair the hormone's thermodynamic stability, self-assembly, and susceptibility to fibrillation. These results thus suggest that, among the 20 natural amino acids, the wild-type Tyr^{B26} best meets the simultaneous challenges of biological activity, protein stability, self-assembly, and protection from toxic misfolding (30). Such co-optimization highlights the multidimensional biophysical and biological landscape of protein evolution.

EXPERIMENTAL PROCEDURES

Preparation of Insulin Analogs—Analogs were made by trypsin catalyzed semi-synthesis using an insulin fragment, *des*-octapeptide[B23-B30]-insulin and modified octapeptides as described (23). The *des*-octapeptide[B23-B30]-insulin was generated *via* cleavage of human insulin with trypsin and purified by reverse-phase high-performance liquid chromatography (HPLC); octapeptides were synthesized by solid-phase synthesis (31). The formation of a peptide bond between Arg^{B22} and a synthetic octapeptide was mediated by trypsin (in a mixed solvent system containing 1,4-butanediol and dimethylacetamide) as previously described (32). Insulin analogs were purified by preparative reverse-phase C4 HPLC (Higgins Analytical Inc., Proto 300 C4 10 μM, 250 x 20 mm), and their purity was assessed by analytical rp-C4 HPLC (Higgins Analytical Inc., Proto 300 C4 5μM, 250 x 4.6 mm). Molecular masses of purified analogs were verified using an Applied Biosystems 4700 proteomics analyzer (matrix-assisted laser-desorption/ionization time-of-flight mass spectrometry; MALDI-TOF MS).

Receptor Binding Assays—Affinities for IR-B were measured by a competitive-displacement scintillation proximity assay. This assay employed detergent-solubilized holo-receptor with C-terminal streptavidin binding protein tags purified by sequential wheat-germ agglutinin (WGA) and Strep-Tactin-affinity chromatography from detergent lysates of polyclonal stably transfected 293PEAK cell lines expressing each receptor. A dilution series of human insulin (a generous gift from Novo-Nordisk A/S, Bagsværd, Denmark) or analog (11 dilutions, 5-fold each with a maximum initial concentration of 2 μM) in 100 μl binding buffer (100 mM HEPES (pH 7.8), 100 mM NaCl, 10 mM $MgSO_4$, 0.025% (v/v) Tween 20 and 0.5% (w/v) bovine serum albumin) was made in a 96-well plate (Costar). The assay was initiated by addition to the wells of a premixed solution containing (i) WGA scintillation-proximity-assay (SPA) beads (Perkin Elmer), (ii) solubilized receptor, and (iii) ^{125}I-Tyr^{A14}-insulin in binding buffer. The final concentration of [^{125}I]-labeled ligand was 7.5 pM, and the amount of receptor added was adjusted so that the extent of labeled ligand binding in the absence of competitor was < 15% of the total added counts in order to avoid ligand-depletion artifacts. Plates were incubated with gentle shaking for 24 h at room temperature, centrifuged, and counted for 5 min/well in a 12-detector Trilux scintillation counter (Perkin Elmer/Wallac). To obtain analog dissociation constants, competitive binding data were analyzed by non-linear regression by the method of Wang (33), a model that provides an analytical solution for the binding of two ligands to a single receptor.

Receptor Binding Screening Protocol—The ability of insulin analogs to displace bound ^{125}I-Tyr^{A14}-insulin from antibody-immobilized WGA-purified receptor was tested at an analog concentration of 0.75 nM. This concentration corresponded to displacement of 95% of receptor-bound ^{125}I-Tyr^{A14}-insulin by the control analog, Orn^{B29}-insulin. The fraction of ^{125}I-Tyr^{A14}-insulin displaced by a given analog permitted assignment to the following three categories: (*low affinity*) <60%, (*intermediate affinity*) 60-80% or (*high affinity*) >80%.

Insulin Self-Assembly—Oligomeric states of the insulin analogs were monitored by size-exclusion chromatography (SEC) using high-performance liquid chromatography (HPLC). The exclusion void volume (V_o) was established with apoferritin (443 kDa). Insulin analogs were made 0.6 mM in a buffer consisting of 25 mM Tris-HCl (pH 7.4), 0.65 mg/ml phenol, 1.6 mg/ml *meta*-cresol, 16 mg/ml glycerol, and $ZnCl_2$ at a ratio of 2 zinc ions per insulin hexamer. For zinc-free conditions, analogs were also made 0.6 mM in phosphate buffered saline, pH 7.4. Protein samples (volume 10 μl) were applied through a Waters 717 autosampler onto a Zenix-C SEC-150 column (Sepax Technologies, Southborough, MA) with nominal fractionation range of 0.5-150 kDa. Proteins were fractionated at a flow rate of 1 ml/min using a Waters Binary HPLC system. Protein elution was monitored at 215 and 280 nm using a dual-lambda Waters 2487 absorbance detector. The mobile phase consisted of 10 mM Tris-HCl (pH 7.4), 140 mM NaCl, with or without 0.3 mM $ZnCl_2$ and 50 mM cyclohexanol; the latter provided a non-aromatic replacement for the phenolic compounds often employed as R_6-hexamer stabilizing- and anti-microbial agents in pharmaceutical formulations (34-36). Data acquisition and processing utilized the Waters HPLC Empower® software. The column was calibrated for apparent molecular-mass determination by fractionating standard proteins individually on the column.

TR Transition and R_6 Co^{2+} kinetic assay—Visible absorption spectroscopy was used to probe the formation and disassembly of phenol-stabilized R_6 Co^{2+}-substituted insulin hexamers. Insulin analogs were made 0.6 mM in a buffer containing 50 mM Tris-HCl (pH 7.4), 50 mM phenol, 0.2 mM $CoCl_2$, and 2 mM NaSCN. Sample pH was readjusted in each case to 7.4, and samples were incubated overnight at room temperature prior to the studies to ensure that a conformational equilibrium was reached. Spectra (400-750 nm) were obtained to monitor tetrahedral Co^{2+} coordination with its signature peak absorption band at 574 nm (37). To assess variation in the amplitude and λ_{max} of the *d-d* transition band, the wild type (WT) spectrum was obtained in four separate preparations containing three replicates each from solutions that were independently prepared; respective standard deviations were ±3.7% and 0.5 nm. To determine the rate of Co^{2+} release from the hexamers, metal ion sequestration was initiated at 25 °C by addition of an aliquot of ethylenediaminetetra-acetic acid (EDTA; 50 mM at pH 7.4) to a final concentration of 2 mM; this yielded a molar ratio of EDTA per formal insulin trimer of 6.7. Attenuation of the 574-nm absorption band was monitored on a timescale of seconds to hours. Post-dissociation absorption spectra (400-750 nm) were collected to confirm complete attenuation of the 574 nm absorption band (38). Kinetic data were fit to mono-exponential decay functions to determine dissociation rate and half-life of Co^{2+} coordinated R_6 hexamers. Independent replicates of the EDTA assay of WT insulin (using freshly prepared stock solutions

in each case) yielded a standard deviation of 15% (±69 sec) in the lifetime.

Circular Dichroism—Far-ultraviolet (UV) CD spectra were obtained on an AVIV spectropolarimeter equipped with an automated syringe-driven titration unit. Wild type insulin or insulin analogs were made 50 μM in 10 mM potassium phosphate (pH 7.4) and 50 mM KCl. Spectra were obtained from 190-250 nm as described (39). Thermodynamic stabilities were probed by guanidine hydrochloride-induced denaturation monitored by CD at helix sensitive wavelength 222 nm. Data were fit by non-linear least squares to a two-state-model (40):

$$\theta(x) = \frac{\theta_A + \theta_B e^{\left(-\Delta G^0_{H_2O} - mx\right)/RT}}{1 + e^{\left(-\Delta G^0_{H_2O} - mx\right)/RT}}$$

where x is the concentration of guanidine hydrochloride, and $\theta_{A,B}$ represent respective estimates of the baseline ellipticities of the protein in its native and unfolded states as extrapolated to a guanidine concentration of 0 M. Baseline values were approximated *via* pre- and post-transition lines represented by equations $\theta_A(x) = \theta_A^{H2O} + m_A x$ and $\theta_B(x) = \theta_B^{H2O} + m_B x$. Such simultaneous fitting avoids artifacts of linear plots of ΔG versus concentration of denaturant (41).

Assessment of Fibril Formation—Insulin or insulin analogs were made 60 μM in phosphate-buffered saline (pH 7.4) containing 0.1% sodium azide and gently rocked at 37 °C in glass vials in the presence of a liquid/air interface. Aliquots were taken at regular intervals and frozen for later analysis of thioflavin T (ThT) fluorescence. The assay was terminated on visual appearance of cloudiness (42). Statistical significance of differences in lag times among analogs was evaluated using Student's t-test.

RESULTS

Receptor-binding studies defined three classes of analogs. 18 insulin analogs containing substitutions at B26 were prepared at small scale (Table 1). To eliminate the B29 tryptic site (and so facilitate semi-synthesis; (43), the analogs each contained Orn^{B29} (in place of Lys^{B29}). Similarly, to provide a basic side chain at B26, an analog was prepared containing both substitutions Orn^{B26} and Orn^{B29}. Cys^{B26}-Orn^{B29}-insulin was not prepared to avoid possible disulfide interchange and/or formation of covalent dimers.

A coarse receptor-binding assay (using IR-B) was first undertaken, which enabled subgroups of the insulin analogs to be distinguished based on displacement of pre-bound ^{125}I-labeled insulin at a uniform analog concentration of 0.75 nM (Fig. 3*A*). At this concentration WT insulin displaced 95% of the prebound tracer (^{125}I-Tyr^{A14}-insulin; see Experimental Procedures). The results defined three classes (Fig. 3*B*): (i) high affinity (tracer displacement >80%; *i.e.*, similar or greater than that observed on binding of WT insulin); (ii) intermediate affinity (tracer displacement 60-80%) and (iii) low affinity (tracer displacement <60%). The low-affinity class contained two aliphatic residues (Ile and Leu). The intermediate-affinity class comprised a diverse set of residues, including Phe, Met, Pro, Thr and Val; the remaining analogs (representing 10 of the 18 analogs tested) were placed in the high-affinity group.

Definitive IR-B binding assays were then undertaken of selected high-, intermediate- and low-affinity analogs (Table 1) using a scintillation proximity assay performed with purified detergent-solubilized receptor isoform expressed in the same cell line. Affinities greater than WT insulin were conferred only by Ser^{B26} and Glu^{B26} (K_d ~ 0.02 nM) whereas the affinities conferred by Tyr^{B26}, Ala^{B26} and Orn^{B26} were indistinguishable (K_d ~ 0.04 nM). The high affinities of Ala^{B26} and Glu^{B26} insulin analogs have previously been reported (3,25). Also in accordance with past studies (22), substitution of Tyr^{B26} by Phe reduced affinity (between two- and threefold). Whereas a similar reduction was conferred by Val^{B26}, substitution of Tyr^{B26} by Ile or Leu led to more severe impairments (by ~10-fold and 30-fold, respectively).

Two sets of observations were particularly striking: (a) the high affinity of analogs containing charged side chains (of either sign) or a short polar side chain (Ser) at B26 and (b) the functional incompatibility of aliphatic substitutions larger than Ala at B26. Although this pattern would in general be unusual on systematic mutagenesis of a conserved aromatic residue in a globular protein (and indeed stands in contrast to results of substitutions at insulin positions Tyr^{B16} and Phe^{B24} (13,16,22), the B26-contacting surface within the μIR complex (4) comprises a shallow solvent-exposed depression at the αCT/L1 junction. Although its structural analysis was limited by low resolution (3.5 Å), this surface contains multiple potential sites for hydrogen bonding and favorable electrostatic interactions, potentially extended by a network of bound water molecules. We speculate that these features of the B26-related surface underlie the enhanced affinities of Ser^{B26} and Glu^{B26} insulin analogs and general exclusion of aliphatic substitutions.

SEC studies provided evidence of decreased or aberrant self-assembly. Competence of the insulin

analogs for zinc-free or zinc-stabilized self-assembly was assessed using a calibrated SEC method (Fig. 4). In the absence of zinc ions, WT insulin was predominantly dimeric as expected at a protein concentration of 0.6 mM under these conditions; the parent Orn^{B29}-insulin analog exhibited similar elution behavior with a slight decrease in extent of dimerization (Fig. 4*A*-*C*). A control for a monomeric insulin analog was provided by insulin *lispro* (KP-insulin; Pro^{B28}→Lys and Lys^{B29}→Pro) (38,44). The elution time of the Orn^{B26} analog is similar to that of KP-insulin. The Glu^{B26} analog exhibits two modes of self-association: *ca*. 40% as dimeric (elution time similar to that of the parent analog) and 60% as a higher-molecular mass aggregate (asterisk in Fig. 4*A*). Although the aberrant elution peak is broad, the mean apparent mass is *ca* 80 kDa, corresponding to 12-14 monomeric units. Perturbed overall dimerization of Glu^{B26}-insulin is in accordance with a previous study by equilibrium ultracentrifugation (3).

SEC studies were extended to conditions of WT R_6 assembly through the addition of zinc ions and phenol (Fig. 4*D*-*F*). To facilitate UV detection of the eluted proteins, cyclohexanol (which is transparent at 215 and 280 nm) was used instead of phenol in the running buffer (see Experimental Procedures). Under these conditions WT insulin and the parent Orn^{B29}-insulin each exhibited an apparent mass slightly larger than a hexamer (43 and 37 kDa, respectively) whereas KP-insulin exhibited an apparent mass of one hexamer (formal molecular mass 35 kDa inclusive of two zinc ions; Fig. 4*F*). The Orn^{B26} analog was predominantly hexameric with slight reduction in apparent mass (33 kDa) whereas the Glu^{B26} analog predominantly exhibited a broad distribution of lower molecular-mass entities (asterisk in Fig. 4*D*). A small percentage of the Glu^{B26} analog (*ca* 5%) eluted as a small bump (41 kDa) on the leading edge of the diffuse profile.

Visible absorption Co^{2+} spectroscopy provided evidence of altered R_6 assembly with accelerated disassembly. The structure and stability of the phenol-stabilized R_6 insulin hexamer may readily be probed by visible absorption spectroscopy on substitution of the zinc ions by Co^{2+} (37). This spectrum exhibits a prominent absorption band due to the tetrahedral coordinate of Co^{2+} in each R_3 trimer of the R_6 hexamer (or in the R^f_3 trimer of a $T_3R^f_3$ hexamer); no such band exists in the spectrum of an octahedral Co^{2+} complex as in the T_3 trimer of an insulin hexamer (or in an EDTA complex) (38). The magnitude of the *d*-*d* band in KP-insulin (*gray* line in Fig. 5*A*) is slightly attenuated relative to the WT hexamer (*black* line), presumed to represent a small shift in the conformational equilibrium from R_6 to $T_3R^f_3$ (37,38,45). The spectrum of the parent Orn^{B29}-insulin (*red* line in Fig. 5*A*) is similar to that of WT insulin whereas the peak signal of the Orn^{B26} analog (*violet*) is attenuated by 7(±1)%. The spectrum of the Glu^{B26} analog (*turquoise)* is attenuated by 39(±2)%, suggesting that the substitution partially impairs the TR transition.

The rate of disassembly of the insulin analog hexamers may likewise be probed through EDTA sequestration of Co^{2+}. This assay's underlying principle exploits transient release of the metal ion when insulin hexamers dissociate and re-assemble within its conformational equilibrium. Because the affinity of EDTA for Co^{2+} is $>10^8$ greater than that of insulin, such transient release results in essentially irreversible sequestration of the metal ion in a colorless complex (38). Whereas the lifetime of the parent hexamer is similar to that of WT insulin (*red* and *black* lines in Fig. 5*B*), the lifetime of the Glu^{B26} hexamer (*turquoise*) was reduced by 2.6(±0.2) fold. Kinetic studies of the Orn^{B26} analog were limited by its progressive precipitation on addition of EDTA. Data collected until the appearance of a visible precipitate displayed an even shorter lifetime (reduced by 15(±3) fold), but interpretation of this value is unclear given the competing aggregation of unknown structure.

CD studies of high-affinity analogs provided evidence of native-like structure with decreased dimerization. Although well tolerated in relation to receptor binding, substitution of Tyr^{B26} by Orn, Glu or Ser was in each case associated with an altered far-UV CD spectrum at a protein concentration of 50 μM (Fig. 6*A*). At this concentration WT insulin and Orn^{B29}-insulin are partially dimeric (46) as assessed by size exclusion chromatography (data not shown). The variant spectra exhibited attenuated ellipticity at 222 nm and deepening of the minimum near 208 nm, spectroscopic features associated with partial loss or dynamic destabilization of α-helices (47). In accordance with the above SEC findings, we ascribe these CD changes to decreased dimerization; analogous CD changes were previously found to accompany dilution of WT insulin in the range 5-100 μM (48), presumably due to enhanced flexibility of the monomer (49-51).

Functional substitutions impair thermodynamic stability. Substitutions Orn^{B26}, Glu^{B26} and Ser^{B26} impaired global stability. Estimates of respective free energies of unfolding (ΔG_u) were obtained at 25 °C based on CD studies of fractional unfolding on chemical denaturation (Fig. 6*B* and histogram in Fig. 6*C*). A trend was observed wherein lower concentrations of denaturant (guanidine hydrochloride)

were required for 50% unfolding of analogs containing the above substitutions (Fig. 6*B* and Table 2, column 3). Application of a two-state model (native and unfolded (40)) yielded ΔG_u values that were in each case at least 0.5 kcal mol^{-1} lower than that of Orn^{B29}-insulin (baseline stability 3.2(±0.1) kcal mol^{-1}). Respective decrements in stability ($\Delta\Delta G_u$) for the Orn^{B26}, Glu^{B26} and Ser^{B26} analogs were 0.7(±0.2), 0.9(±0.2) and 0.9(±0.2) kcal mol^{-1}. Such perturbations were thus similar to that reported in studies of an insulin analog containing substitution of Phe^{B24} by Ala ($\Delta\Delta G_u$ 0.8(±0.2) kcal mol^{-1} (52)).

The *m*-values obtained in the fitting (which correlate with extent of solvation of nonpolar surfaces on protein denaturation (40)) were significantly attenuated relative to Orn^{B29}-insulin or WT insulin (column 4 in Table 2). Such attenuation suggests that in their respective native states, the analogs exhibit less efficient desolvation of nonpolar surfaces. This trend may be due to a direct perturbation of the (A2, A3)-related inter-chain crevice (2) by Orn^{B26}, Glu^{B26} and Ser^{B26}; transmitted structural perturbations cannot be excluded.

Functional substitutions led to accelerated fibrillation. The reduced stabilities, impaired dimerization and perturbed *m*-values of the Orn^{B26}, Glu^{B26} and Ser^{B26} analogs motivated assessment of lag times prior to onset of fibrillation relative to Orn^{B29}-insulin (Fig. 6*D* and column 5 in Table 2). These assays were performed in the absence of zinc ions. Although Orn^{B29}-insulin exhibited a broad range of lag times greater than 5 days (with a mean of 13 days in N = 14 trials), the analogs consistently exhibited lag times less than 4 days (N = 3). Despite the small sample size, *p*-values were < 0.01 for each analog. These trends are therefore unrelated to the charge of the B26 side chain and net charge of the protein (53). We speculate that perturbation of the (A2, A3)-related inter-chain crevice favors local unfolding (42) and non-native conformational excursions, in turn favoring formation of an amyloidogenic nucleus (Fig. 7*C*) (54).

DISCUSSION

Vertebrate insulin sequences exhibit broad conservation (17), including several invariant residues recently shown to pack at the primary hormone-receptor interface (4). Examples are provided by Val^{A3}, Val^{B12} and Phe^{B24}, non-polar side chains of distinctive shape and size whose respective binding sites in the IR are also invariant (7). Such framework contacts are also conserved among IGFs and the cognate IGF-1R (20,21). Diverse amino-acid substitutions at A3, B12, B24 or B25 impair receptor binding, including mutations as subtle as Val^{A3}→Leu, Val^{B12}→Leu, Phe^{B24}→Tyr or Phe^{B24}→Leu (13,55-57). Co-evolution of the hormone-receptor interface has presumably led to the strict conservation of such contact sites. Although current co-crystal structures of model insulin-μIR complexes were obtained at low resolution (3.5 Å; (4), we anticipate that future improvements in resolution may enable quantitative rationalization of such classical structure-activity relationships.

Systematic mutagenesis of the insulin surface. Mutational surveys of key residues in insulin through systematic synthesis of all possible substitutions has provided broad insight into structure-activity relationships (58,59). Such surveys may complement crystallographic studies of "micro-receptor" complexes (4), especially as to date such fragments lack the FnIII domains in the IR α-subunit and so provide an incomplete description of the hormone-receptor interface. A mutational survey of Glu^{B13}, for example, has suggested that this side chain contacts the IR (59) despite its lack of contact to αCT or L1 (4); this inference is in accordance with a proposed Site 2 contact within a FnIII domain (6,60). Mutational surveys may also provide insight into conserved contacts visualized within the μIR complex. We have recently utilized this approach to survey mutations at position B24 (16). The results provided a probe of a deep nonpolar pocket within the hormone-μIR complex (4). At this site only the native side chain of Phe^{B24} among *natural* amino acids confers high activity. The non-standard aliphatic residue cyclohexanylalanine (Cha^{B24}) was found to be compatible with high activity, demonstrating that aromaticity *per se* is not required within the B24-related pocket (16).

Structure-activity relationships at B26. Because the low resolution of the present μIR co-crystal structure (4) and enigmatic structure-activity relationships in prior studies (23-29), we undertook a systematic mutagenesis of the B26 position with all standard amino acids—with the exceptions of Cys (to avoid a disulfide exchange), Lys and Arg (to avoid tryptic cleavage of the octapeptide in the course of semi-synthesis; see Experimental Procedures). The latter two residues were represented by the basic amino acid Orn, an analog resistant to tryptic cleavage. The analogs also contained Orn^{B29} in place of the native Lys for the same reason. Semi-synthesis thus enabled rapid and efficient introduction of diverse substitutions at B26 without encountering barriers to recombinant protein expression (24).

The present B26 survey has demonstrated—in striking contrast to our prior B24 survey (16)—that chemically diverse side chains are functional whereas side chains associated with impaired IR binding were hydrophobic (Ile^{B26}, Leu^{B26} and Pro^{B26}). Trp^{B26} and Phe^{B26} were compatible with near WT affinities, suggesting that their "weakly polar" electronic characteristics or planarity (each feature a consequence of aromaticity (61)) are favorable at the B26-related μIR surface. The displaced conformation of residues B24-B27 in the μIR complex leaves Tyr^{B26} partially exposed at a solvated edge of the L1 domain (Fig. 2*B*). The reduced activity of Pro^{B26}-Orn^{B29}-insulin may reflect not only its non-polarity but also its constrained and distinctive conformation.

All of the tested polar or charged amino acids conferred substantial activity (Asp, Glu, His, Asn, Orn, Gln, Ser and the native Tyr; with Thr in the intermediate class). Of these, the highest affinities were conferred by Glu, Ser, Orn and the native Tyr. Indeed Glu^{B26} and Ser^{B26} analogs of Orn^{B29}-insulin exhibited IR affinities twofold greater than those of WT insulin or Orn^{B29}-insulin itself; the affinity of Orn^{B26}-Orn^{B29}-insulin was indistinguishable from WT. *Yet, Glu, Ser and Lys (by analogy to Orn) are rarely found in nature as alternatives for Tyr^{B26}*. To investigate this seeming evolutionary paradox, we measured free energies of unfolding (ΔG_u) by chemical denaturation (40). The thermodynamic stabilities of these active variants were each markedly reduced relative to WT insulin or its parent control ($\Delta\Delta G_u$ 0.9(±0.2), 0.9(±0.2) and 0.7(±0.2) kcal mol^{-1}, respectively.) In SEC studies the Glu^{B26} and Orn^{B26} analogs exhibited impaired zinc-free dimerization and zinc-stabilized hexamer formation in accordance with the classical packing of Tyr^{B26} at an aromatic-rich dimer interface (2). Whereas decreased dimerization of Glu^{B26}-insulin has previously been reported (3), the SEC data also demonstrated aberrant higher-order zinc-independent aggregation together with instability of the R_6 zinc hexamer. Further, this substitution and Orn^{B26} perturbed the kinetic stability of the R_6 Co^{2+}-substituted insulin hexamer. Finally, we observed that the high-affinity analogs each exhibited (under zinc-free conditions) markedly reduced lag times prior to fibril formation. Susceptibility to such aggregation-coupled misfolding would be expected to be further magnified by impaired native self-assembly.

The present set of analogs contained the platform substitution Lys^{B29}→Orn, introduced to simplify the protocol of trypsin-mediated semi-synthesis). This non-standard residue (related to Lys by removal of a single methylene moiety from a linear side chain; *i.e.*, [2, 5]-diaminopentanoic acid *versus* [2, 6]-diaminohexanoic acid) does not perturb the activity or stability of insulin. Its use as a template was unlikely to have influenced the pattern of activities among B26 analogs. Indeed, to the extent that our survey of substitutions recapitulated prior studies of particular analogs in a native context (such as Ala^{B26}-insulin and Glu^{B26}-insulin), similar results were obtained with respect to activity (23) and self-assembly (3). Such template independence is not surprising in this case as residue B29 is peripheral to the hormone's receptor-binding surface (62,63), does not contribute to classical self-association surfaces (2,64) and is not conserved among vertebrate insulin sequences (17). Further, in several otherwise high-resolution crystal structures of insulin, the side chain of Lys^{B29} exhibits high thermal *B* factors (2) and/or lacks continuous electron density (in particular toward its distal end), suggesting dynamic disorder (as exemplified by Protein Databank entries 1BEN, 1EV3, 1TRZ^2 (65-67); such flexibility is in accordance with motional narrowing of ^{1}H-NMR resonances observed in a variety of NMR studies (49,68). In pharmacologic applications these considerations have favored B29 as a site of substitution or chemical modification (*e.g.*, Pro^{B29} in Humalog®, Glu^{B29} in Apidra®, and acylation of Lys^{B29} in Levemir® and Tresiba®; Ref 69-72). Surprisingly, the platform substitution Lys^{B29}→Orn (introduced only to simplify the protocol of trypsin-mediated semi-synthesis) was itself associated with enhanced resistance to fibrillation at neutral pH, a finding that suggests that the mechanism of amyloid formation can be influenced by subtle changes—despite its seeming universality among polypeptide sequences (30). It is possible that long-range electrostatic interactions by the δ-amino group of Orn^{B29} (made more distant and so weakened as compared to the ε-amino group of Lys^{B29}) may impose kinetic barriers to partial transient unfolding as envisioned in a putative amyloidogenic intermediate (73). Interpretation of relative fibrillation lag times is limited by the lack of structural information pertaining to such non-native intermediates.

Interest in position B26 has recently been renewed by evidence that substitution of Tyr^{B26} by Asn (and possibly other amino acids) can alter the ratio of affinities to isoform IR-A *versus* IR-B in cellular assays, possibly as a consequence of a B26-related conformational change (74). Although the degree of selectivity was small, such studies motivated elegant use of non-standard protein engineering to create a novel class of constrained analogs (75). The latter studies employed cells lines that respectively expressed

either one isoform or the other, but in different lineage-specific contexts. Since such membranes may differ in composition or proteome, it would be of future interest to investigate whether such isoform selectivity might be observed in studies of purified receptor isoforms (as distinct from intact cells), and if so, might extend to receptor fragments (such as the μIR model).

It would be of future interest to investigate the solution structures of selected B26 analogs by NMR spectroscopy. Although such studies would ordinarily require use of a monomeric insulin template (such as insulin *lispro* (76)) to circumvent insulin self-association—a confounding issue at the high protein concentrations required for NMR—our SEC studies of Orn^{B26}-Orn^{B29}-insulin and Glu^{B26}-Orn^{B29}-insulin suggest that these analogs may be amenable to high-resolution study without further modification. Of particular interest would be the extent to which these B26 substitutions may lead to nonlocal changes in the dynamics of the hormone's α-helical domain (such as in its pattern of conformational broadening (77)) due to perturbation of the Ile^{A2}/Val^{A3}-associated inter-chain crevice. In light of the displaced conformation of the B23-B27 segment in the μIR complex (4), it would be of further interest to probe whether such B26 substitutions weaken the attachment of this segment to the insulin core. A recent study of the insulin monomer by molecular-dynamics simulations has predicted that long-range interactions by Tyr^{B26} in WT insulin regulate transient detachment and re-attachment of this segment through a series of transient conformational substates (78). Use of heteronuclear NMR methods to uncover such "excited-state" conformations represents a promising frontier of protein science (79).

Toxic misfolding as an evolutionary constraint. Although *in vivo* formation of insulin fibrils is rare in humans, a hystricomorph rodent in South America (*Octodon degus*) develops senile diabetes mellitus mostly in association with deposition of an amyloid strictly composed of insulin in its islets of Langerhans (80,81). The insulin sequence in this rodent contains the unusual substitution His^{B10}→Asn, which removes the central Zn^{2+} coordination site in the classical insulin hexamer. In addition, the variant insulin of *Octodon degus* contains substitution Tyr^{B26}→Arg, which would further be expected to impair or block hexamer assembly. Because the self-assembly of Zn^{2+}-insulin hexamers is thought to protect the insulin from partial unfolding and non-native aggregation within the storage granules of pancreatic β-cells (1), the combined adverse effects of Asn^{B10} and Arg^{B26} on self-assembly may provide a molecular mechanism for the formation of an insulin-specific amyloid in this species. Such an experiment of nature highlights in the breach the implicit constraint that we propose underlies the broad conservation of Tyr at B26: avoidance of toxic misfolding. We thus envisage that a combination of inefficient or unstable disulfide pairing, perturbed hexamer assembly, and heightened susceptibility to fibrillation might be associated with a risk of toxic protein deposition as an amyloidogenic disease and so impose independent evolutionary constraints (Fig. 7*A*) (68). The displacement of the C-terminal segment of the B chain from the hormone's α-helical core (Fig. 7*B*) would otherwise favor a mechanism of fibrillation based on distortion of the monomeric structure with aberrant exposure of nonpolar surfaces (Fig. 7*C*) (53).

Although residue B26 is broadly conserved as Tyr among vertebrate insulins and as Phe among IGFs (17), such conservation is not strict. In addition to the amyloidogenic *Octodon degus* sequence, for example, several hystricomorph insulins contain Arg or Ser at B26 (17). Further, the genome of *Poecilia formosa* (the Amazon molly fish) encodes a proinsulin/IGF-like protein wherein the B24-B26 segment contains a non-aromatic residue at B26 (Phe^{B24}-Tyr^{B26}-Asn^{B26}; SwissProt entry A0A096M678_POEFO). Such anomalies are in accordance with the dispensability of Tyr^{B26} in truncated insulin analogs with native activity, as exemplified by *des*-pentapeptide[B26-B30]-insulin-amide insulin (26). It is possible that the life spans of such animals are shorter than the time scale of toxic protein deposition, and so their reproductive success is unaffected by the variant insulin.

Concluding Remarks. Our results suggest that conservation of Tyr^{B26} is unlikely to be enjoined by the topography of the IR. The reduced stability of alternative high-affinity analogs and their enhanced susceptibility to fibrillation instead suggest that its conservation reflects co-optimization of several factors—not only activity, but also stability and avoidance of toxic misfolding (30). The latter's evolutionary importance is highlighted by the monogenic proinsulin syndrome (82). Indeed, the broad conservation of Tyr^{B26} may reflect the multiple roles played by specific side chains in the course of a complex "conformational life cycle" from nascent folding to receptor binding. It would be of future interest to extend our survey from insulin to proinsulin in relation to foldability in the endoplasmic reticulum and corresponding folding efficiency *in vitro*.

Acknowledgments. We thank Drs Q.-X. Hua, W. Jia, S. H. Nakagawa, and Z.-l Wan for advice regarding experimental procedures; J. Racca for assistance with figures; and Profs P. Arvan, T. L. Blundell, M. Karplus, P. G. Katsoyannis and M. Liu for general discussion. VP and NR were supported by a predoctoral fellowship of the CWRU Medical Scientist Training Program supported by institutional National Institutions of Heath grant T32 GM007250 and individual NIH fellowship F30 DK094685-04. NBF and JW were supported in part by the American Diabetes Association. This work was supported in part by grants from the National Institute of Diabetes, Digestive and Kidney Diseases R01 DK04949 and DK079233 (MAW) and from the Australian National Health and Medical Research Council (NHMRC) Project Grants 1005896 and 1058233 and the Hazel and Pip Appel Fund (to MCL). MCL also acknowledges NHMRC Independent Research Institutes Infrastructure Support Scheme Grant 361646 and Victorian State Government Operational Infrastructure Support Grant (to the Walter and Eliza Hall Institute). The authors dedicate this article to the memory of the late Prof. Donald F. Steiner (University of Chicago).

Disclosure of Competing Interests. MAW has equity in Thermalin Diabetes, LLC (Cleveland, OH) where he serves as Chief Scientific Officer; he has also been consultant to Merck Research Laboratories and DEKA Research & Development Corp. NBP and JW are consultants to Thermalin Diabetes, LLC. Part of MCL's research is funded by Sanofi (Germany).

Author Contributions. VP coordinated the paper, analyzed the data as well as obtained the fibril and guanidine titration studies. NBP provided SEC-HPLC data as well as provided important input to the paper. NR carried out experiments related to the cobalt coordinated insulin hexamers. MCL provided substantial input regarding the interactions with the insulin receptor. JW provided data for the receptor binding experiments. MAW conceived the paper and also provided the lab space for much of the experiments described herein.

REFERENCES

1. Dodson, G., and Steiner, D. (1998) The role of assembly in insulin's biosynthesis. *Curr Opin Struct Biol.* **8**, 189-194
2. Baker, E. N., Blundell, T. L., Cutfield, J. F., Cutfield, S. M., Dodson, E. J., Dodson, G. G., Hodgkin, D. M., Hubbard, R. E., Isaacs, N. W., and Reynolds, C. D. (1988) The structure of 2Zn pig insulin crystals at 1.5 Å resolution. *Philos Trans R Soc Lond B Biol Sci.* **319**, 369-456
3. Brange, J., Ribel, U., Hansen, J. F., Dodson, G., Hansen, M. T., Havelund, S., Melberg, S. G., Norris, F., Norris, K., and Snel, L. (1988) Monomeric insulins obtained by protein engineering and their medical implications. *Nature.* **333**, 679-682
4. Menting, J. G., Yang, Y., Chan, S. J., Phillips, N. B., Smith, B. J., Whittaker, J., Wickramasinghe, N. P., Whittaker, L., Pandyarajan, V., Wan, Z., Yadav, S. P., Carroll, J. M., Srokes, N., Roberts, C. T., Ismail-Beigi, F., Milewski, M., Steiner, D., Chauhan, V., Ward, C., Weiss, M. A., and Lawrence, M. C. (2014) A structural hinge in insulin enables its receptor engagement. *Proc Natl Acad Sci U S A.* **111**, 1-48
5. Moller, D. E., Yokota, A., Caro, J. F., and Flier, J. S. (1989) Tissue-specific expression of two alternatively spliced insulin receptor mRNAs in man. *Mol Endocrinol.* **3**, 1263-1269
6. De Meyts, P., and Whittaker, J. (2002) Structural biology of insulin and IGF1 receptors: implications for drug design. *Nat Rev Drug Discov.* **1**, 769-783
7. Ward, C. W., Menting, J. G., and Lawrence, M. C. (2013) The insulin receptor changes conformation in unforeseen ways on ligand binding: Sharpening the picture of insulin receptor activation. *Bioessays*. **35**, 945-954
8. Hubbard, S. R. (1997) Crystal structure of the activated insulin receptor tyrosine kinase in complex with peptide substrate and ATP analog. *EMBO J.* **16**, 5572-5581
9. Cabail, M. Z., Li, S., Lemmon, E., Bowen, M. E., Hubbard, S. R., and Miller, W.T. (2015) The insulin and IGF1 receptor kinase domains are functional dimers in the activated state. *Nat Commun.* **6:6406**
10. Lou, M., Garrett, T. P., McKern, N. M., Hoyne, P. A., Epa, V. C., Bentley, J. D., Lovrecz, G. O., Cosgrove, L. J., Frenkel, M. J., and Ward, C. W. (2006) The first three domains of the insulin receptor differ structurally from the insulin-like growth factor 1 receptor in the regions governing ligand specificity. *Proc Natl Acad Sci U S A.* **103**, 12429-12434
11. Garrett, T. P., McKern, N. M., Lou, M., Frenkel, M. J., Bentley, J. D., Lovrecz, G. O., Elleman, T. C., Cosgrove, L. J., and Ward, C. W. (1998) Crystal structure of the first three domains of the type-1 insulin-like growth factor receptor. *Nature*. **394**, 395-399
12. Croll, T., Smith, B. J., Whittaker, J., Margetts, M. B., Weiss, M. A., Ward, C. W., and Lawrence, M. C. (2016) Higher-resolution structure of the human insulin receptor ectodomain: multi-modal inclusion of the insert domain. *Structure*. **24**, 469-76
13. Mirmira, R. G., Nakagawa, S. H., and Tager, H. S. (1991) Importance of the character and configuration of residues B24, B25, and B26 in insulin-receptor interactions. *J Biol Chem.* **266**, 1428-1436
14. Hua, Q. X., Shoelson, S. E., Kochoyan, M., and Weiss, M. A. (1991) Receptor binding redefined by a structural switch in a mutant human insulin. *Nature.* **354**, 238-241
15. Xu, B., Huang, K., Chu, Y. C., Hu, S. Q., Nakagawa, S., Wang, S., Wang, R. Y., Whittaker, J., Katsoyannis, P. G., and Weiss, M. A. (2009) Decoding the cryptic active conformation of a protein by synthetic photoscanning: Insulin inserts a detachable arm between receptor domains. *J Biol Chem.* **284**, 14597-14608
16. Pandyarajan, V., Smith, B. J., Phillips, N. B., Whittaker, L., Cox, G. P., Wickramasinghe, N., Menting, J. G., Wan, Z.-l., Whittaker, J., and Ismail-Beigi, F. (2014) Aromatic Anchor at an

Invariant Hormone-Receptor Interface FUNCTION OF INSULIN RESIDUE B24 WITH APPLICATION TO PROTEIN DESIGN. *J Biol Chem.* **289**, 34709-34727
17. Conlon, J. M. (2001) Evolution of the insulin molecule: insights into structure-activity and phylogenetic relationships. *Peptides.* **22**, 1183-1193
18. Shoelson, S. E., Lee, J., Lynch, C. S., Backer, J. M., and Pilch, P. F. (1993) Bpa^{B25} insulins. Photoactivatable analogues that quantitatively cross-link, radiolabel, and activate the insulin receptor. *J Biol Chem.* **268**, 4085-4091
19. Kurose, T., Pashmforoush, M., Yoshimasa, Y., Carroll, R., Schwartz, G. P., Burke, G. T., Katsoyannis, P. G., and Steiner, D. F. (1994) Cross-linking of a B25 azidophenylalanine insulin derivative to the carboxyl-terminal region of the α-subunit of the insulin receptor. Identification of a new insulin-binding domain in the insulin receptor. *J Biol Chem.* **269**, 29190-29197
20. Rinderknecht, E., and Humbel, R. E. (1978) The amino acid sequence of human insulin-like growth factor I and its structural homology with proinsulin. *J Biol Chem.* **253**, 2769-2776
21. Rinderknecht, E., and Humbel, R. E. (1978) Primary structure of human insulin-like growth factor II. *FEBS Lett.* **89**, 283-286
22. Hu, S.-q., Burke, G. T., and Katsoyannis, P. G. (1993) Contribution of the B16 and B26 tyrosine residues to the biological activity of insulin. *J Protein Chem.* **12**, 741-747
23. Inouye, K., Watanabe, K., Tochino, Y., Kobayashi, M., and Shigeta, Y. (1981) Semisynthesis and properties of some insulin analogs. *Biopolymers.* **20**, 1845-1858
24. Kristensen, C., Kjeldsen, T., Wiberg, F. C., Schaffer, L., Hach, M., Havelund, S., Bass, J., Steiner, D. F., and Andersen, A. S. (1997) Alanine scanning mutagenesis of insulin. *J Biol Chem.* **272**, 12978-12983
25. Chen, H., Shi, M., Guo, Z. Y., Tang, Y. H., Qiao, Z. S., Liang, Z. H., and Feng, Y. M. (2000) Four new monomeric insulins obtained by alanine scanning the dimer-forming surface of the insulin molecule. *Protein Eng.* **13**, 779-782
26. Cosmatos, A., Ferderigos, N., and Katsoyannis, P. G. (1979) Chemical synthesis of [*des*(tetrapeptide B^{27-30}), $Tyr(NH_2)^{26}$-B] and [*des*(pentapeptide B^{26-30}), $Phe(NH_2)^{25}$-B] bovine insulins. *Int J Pept Protein Res.* **14**, 457-471
27. Fischer, W. H., Saunders, D., Brandenburg, D., Wollmer, A., and Zahn, H. (1985) A shortened insulin with full *in vitro* potency. *Biol Chem Hoppe Seyler.* **366**, 521-525
28. Žáková, L., Kazdová, L., Hančlová, I., Protivínská, E., Šanda, M., Buděšínský, M., and Jiráček, J. (2008) Insulin analogues with modifications at position B26. Divergence of binding affinity and biological activity. *Biochemistry.* **47**, 5858-5868
29. Jiracek, J., Zakova, L., Antolikova, E., Watson, C. J., Turkenburg, J. P., Dodson, G. G., and Brzozowski, A. M. (2010) Implications for the active form of human insulin based on the structural convergence of highly active hormone analogues. *Proc Natl Acad Sci U S A.* **107**, 1966-1970
30. Dobson, C. M. (2003) Protein folding and misfolding. *Nature*. **426**, 884-890
31. Barany, G., and Merrifield, R. B. (1980). in *The Peptides* (Gross, E., and Meienhofer, J. eds.), Academic Press, New York. pp 273-284
32. Kubiak, T., and Cowburn, D. (1986) Enzymatic semisynthesis of porcine despentapeptide (B26-30) insulin using unprotected desoctapeptide (B23-30) insulin as a substrate. *Int J Pept Protein Res.* **27**, 514-521
33. Wang, Z. X. (1995) An exact mathematical expression for describing competitive binding of two different ligands to a protein molecule *FEBS Lett.* **360**, 111-114
34. Derewenda, U., Derewenda, Z., Dodson, E. J., Dodson, G. G., Reynolds, C. D., Smith, G. D., Sparks, C., and Swenson, D. (1989) Phenol stabilizes more helix in a new symmetrical zinc insulin hexamer. *Nature.* **338**, 594-596

35. Brange, J. (ed) (1987) *Galenics of Insulin: The Physico-chemical and Pharmaceutical Aspects of Insulin and Insulin Preparations*, Vol. , Springer Berlin Heidelberg, Berlin
36. Brange, J. (2000) Physical stability of proteins. in *Pharmaceutical formulation development of peptides and proteins* (Frokjaer, S., and Hovgaard, L. eds.), 1st Ed., Taylor & Francis, Philadelphia, PA, USA. pp 89-109
37. Roy, M., Brader, M. L., Lee, R. W., Kaarsholm, N. C., Hansen, J. F., and Dunn, M. F. (1989) Spectroscopic signatures of the T to R conformational transition in the insulin hexamer. *J Biol Chem.* **264**, 19081-19085
38. Birnbaum, D. T., Kilcomons, M. A., DeFelippis, M. R., and Beals, J. M. (1997) Assembly and dissociation of human insulin and $Lys^{B28}Pro^{B29}$-insulin hexamers: a comparison study. *Pharm Res.* **14**, 25-36
39. Sreerama, N., and Woody, R. W. (1993) A self-consistent method for the analysis of protein secondary structure from circular dichroism. *Anal Biochem.* **209**, 32-44
40. Sosnick, T. R., Fang, X., and Shelton, V. M. (2000) Application of circular dichroism to study RNA folding transitions. *Methods Enzymol.* **317**, 393-409
41. Pace, C. N., and Shaw, K. L. (2000) Linear extrapolation method of analyzing solvent denaturation curves. *Proteins.* **Suppl 4**, 1-7
42. Yang, Y., Petkova, A., Huang, K., Xu, B., Hua, Q. X., Ye, I. J., Chu, Y. C., Hu, S. Q., Phillips, N. B., Whittaker, J., Ismail-Beigi, F., Mackin, R. B., Katsoyannis, P. G., Tycko, R., and Weiss, M. A. (2010) An Achilles' Heel in an amyloidogenic protein and its repair. Insulin dynamics, misfolding, and therapeutic design. *J Biol Chem.* **285**, 10806-10821
43. Izumiya, N., Okazaki, H., Matsumoto, I., and Takiguchi, H. (1959) Action of trypsin and papain on derivatives of diaminobutyric acid, ornithine and lysine. *J Biochem.* **46**, 1347-1354
44. Campbell, R. K., Campbell, L. K., and White, J. R. (1996) Insulin lispro: its role in the treatment of diabetes mellitus. *Ann Pharmacother.* **30**, 1263-1271
45. Ciszak, E., Beals, J. M., Frank, B. H., Baker, J. C., Carter, N. D., and Smith, G. D. (1995) Role of C-terminal B-chain residues in insulin assembly: the structure of hexameric $Lys^{B28}Pro^{B29}$-human insulin. *Structure.* **3**, 615-622
46. Attri, A. K., Fernandez, C., and Minton, A. P. (2010) pH-dependent self-association of zinc-free insulin characterized by concentration-gradient static light scattering. *Biophys Chem.* **148**, 28-33
47. Yang, J. T., Wu, C. S., and Martinez, H. M. (1986) Calculation of protein conformation from circular dichroism. *Methods Enzymol.* **130**, 208-251
48. Pocker, Y., and Biswas, S. B. (1980) Conformational dynamics of insulin in solution. Circular dichroic studies. *Biochemistry.* **19**, 5043-5049
49. Jacoby, E., Hua, Q. X., Stern, A. S., Frank, B. H., and Weiss, M. A. (1996) Structure and dynamics of a protein assembly. ^{1}H-NMR studies of the 36 kDa R_6 insulin hexamer. *J Mol Biol.* **258**, 136-157
50. Hua, Q. X., Ladbury, J. E., and Weiss, M. A. (1993) Dynamics of a monomeric insulin analogue: testing the molten-globule hypothesis. *Biochemistry.* **32**, 1433-1442
51. Zoete, V., Meuwly, M., and Karplus, M. (2004) A comparison of dynamic behavior of monomeric and dimeric insulin shows structural rearrangements in the active monomer. *J Mol Biol.* **342**, 913-929
52. Hua, Q. X., Xu, B., Huang, K., Hu, S. Q., Nakagawa, S., Jia, W., Wang, S., Whittaker, J., Katsoyannis, P. G., and Weiss, M. A. (2009) Enhancing the activity of insulin by stereospecific unfolding. Conformational life cycle of insulin and its evolutionary origins. *J Biol Chem.* **284**, 14586-14596
53. Nielsen, L., Frokjaer, S., Brange, J., Uversky, V. N., and Fink, A. L. (2001) Probing the mechanism of insulin fibril formation with insulin mutants. *Biochemistry.* **40**, 8397-8409

54. Jimenez, J. L., Nettleton, E. J., Bouchard, M., Robinson, C. V., Dobson, C. M., and Saibil, H. R. (2002) The protofilament structure of insulin amyloid fibrils. *Proc Natl Acad Sci U S A.* **99**, 9196-9201
55. Kobayashi, M., Ohgaku, S., Iwasaki, M., Maegawa, H., Shigeta, Y., and Inouye, K. (1982) Characterization of [Leu^{B24}]- and [Leu^{B25}]-insulin analogues. Receptor binding and biological activity. *Biochem J.* **206**, 597-603
56. Kobayashi, M., Takata, Y., Ishibashi, O., Sasaoka, T., Iwasaki, T. M., Shigeta, Y., and Inouye, K. (1986) Receptor binding and negative cooperativity of a mutant insulin, [LeuA3]-insulin. *Biochem Biophys Res Commun.* **137**, 250-257
57. Hu, S. Q., Burke, G. T., Schwartz, G. P., Ferderigos, N., Ross, J. B., and Katsoyannis, P. G. (1993) Steric requirements at position B12 for high biological activity in insulin. *Biochemistry.* **32**, 2631-2635
58. Weiss, M. A., Hua, Q. X., Jia, W., Nakagawa, S. H., Chu, Y. C., and Katsoyannis, P. G. (2002) Activities of insulin analogues at position 8 are uncorrelated with thermodynamic stability. in *Insulin and Related Proteins - Structure to Function and Pharmacology* (Dieken, M. L., Federwisch, M., and De Meyts, P. eds.), Kluwar Academic Publishers, Dordrecht, The Netherlands. pp 103-119
59. Glendorf, T., Sorensen, A. R., Nishimura, E., Pettersson, I., and Kjeldsen, T. (2008) Importance of the solvent-exposed residues of the insulin B chain α-helix for receptor binding. *Biochemistry.* **47**, 4743-4751
60. De Meyts, P. (1994) The structural basis of insulin and insulin-like growth factor-I receptor binding and negative co-operativity, and its relevance to mitogenic versus metabolic signaling. *Diabetologia.* **37**, S135-S148
61. Burley, S. K., and Petsko, G. A. (1988) Weakly polar interaction in proteins. *Adv Protein Chem.* **39**, 125-189
62. De Meyts, P., and Whittaker, J. (2002) Structure-function relationships of insulin and insulin-like growth factor-I receptor binding. in *Insulin and Other Proteins. From Structure to Function and Pharmacology* (De Meyts, P., Dieken, M. L., and Federwisch, M. eds.), Kluwer Publishing, Dordrecht, the Netherlands. pp 131-149
63. Menting, J. G., Whittaker, J., Margetts, M. B., Whittaker, L. J., Kong, G. K., Smith, B. J., Watson, C. J., Zakova, L., Kletvikova, E., Jiráček, J., Chan, S. J., Steiner, D. F., Dodson, G. G., Brzozowski, A. M., Weiss, M. A., Ward, C. W., and Lawrence, M. C. (2013) How insulin engages its primary binding site on the insulin receptor. *Nature.* **493**, 241-245
64. Blundell, T. L., Cutfield, J. F., Cutfield, S. M., Dodson, E. J., Dodson, G. G., Hodgkin, D. C., Mercola, D. A., and Vijayan, M. (1971) Atomic positions in rhombohedral 2-zinc insulin crystals. *Nature.* **231**, 506-511
65. Smith, G. D., Ciszak, E., and Pangborn, W. (1996) A novel complex of a phenolic derivative with insulin: Structural features related to the T→ R transition. *Protein Sci.* **5**, 1502-1511
66. Smith, G. D., Ciszak, E., Magrum, L. A., Pangborn, W. A., and Blessing, R. H. (2000) R_6 hexameric insulin complexed with m-cresol or resorcinol. *Acta Crystallogr D Biol Crystallogr.* **56**, 1541-1548
67. Ciszak, E., and Smith, G. D. (1994) Crystallographic evidence for dual coordination around zinc in the T_3R_3 human insulin hexamer. *Biochemistry.* **33**, 1512-1517
68. Jørgensen, A. M., Kristensen, S. M., Led, J. J., and Balschmidt, P. (1992) Three-dimensional solution structure of an insulin dimer. A study of the B9(Asp) mutant of human insulin using nuclear magnetic resonance, distance geometry and restrained molecular dynamics. *J Mol Biol.* **227**, 1146-1163
69. Hirsch, I. B. (2005) Insulin analogues. *N Engl J Med.* **352**, 174-183

70. Garg, S. K., Ellis, S. L., and Ulrich, H. (2005) Insulin glulisine: a new rapid-acting insulin analogue for the treatment of diabetes. *Expert Opin Pharmacother.* **6**, 643-651
71. Goldman-Levine, J. D., and Lee, K. W. (2005) Insulin detemir -- a new basal insulin analog. *Ann Pharmacother.* **39**, 502-507
72. Keating, G. M. (2013) Insulin degludec and insulin degludec/insulin aspart: a review of their use in the management of diabetes mellitus. *Drugs* **73**, 575-593
73. Fink, A. L. (2005) Natively unfolded proteins. *Curr Opin Struct Biol.* **15**, 35-41
74. Zakova, L., Kletvikova, E., Lepsik, M., Collinsova, M., Watson, C. J., Turkenburg, J. P., Jiracek, J., and Brzozowski, A. M. (2014) Human insulin analogues modified at the B26 site reveal a hormone conformation that is undetected in the receptor complex. *Acta Crystallogr D Biol Crystallogr.* **70**, 2765-2774
75. Viková, J., Collinsová, M., Kletvíková, E., Buděšínský, M., Kaplan, V., Žáková, L., Veverka, V., Hexnerová, R., Aviñó, R. J. T., and Straková, J. (2016) Rational steering of insulin binding specificity by intra-chain chemical crosslinking. *Sci Rep.* **6**, 19431
76. Hua, Q. X., Jia, W., and Weiss, M. A. (2011) Conformational dynamics of insulin. *Front Endocrinol (Lausanne).* **2,** 48
77. Hua, Q. X., Hu, S. Q., Frank, B. H., Jia, W., Chu, Y. C., Wang, S. H., Burke, G. T., Katsoyannis, P. G., and Weiss, M. A. (1996) Mapping the functional surface of insulin by design: structure and function of a novel A-chain analogue. *J Mol Biol.* **264**, 390-403
78. Papaioannou, A., Kuyucak, S., and Kuncic, Z. (2015) Molecular Dynamics Simulations of Insulin: Elucidating the Conformational Changes that Enable Its Binding. *PLoS One.* **10**, e0144058
79. Mulder, F. A., Mittermaier, A., Hon, B., Dahlquist, F. W., and Kay, L. E. (2001) Studying excited states of proteins by NMR spectroscopy. *Nat Struct Biol.* **8**, 932-935
80. Nishi, M., and Steiner, D. F. (1990) Cloning of complementary DNAs encoding islet amyloid polypeptide, insulin, and glucagon precursors from a New World rodent, the degu, *Octodon degus*. *Mol Endocrinol.* **4**, 1192-1198
81. Hellman, U., Wernstedt, C., Westermark, P., O'Brien, T. D., Rathbun, W. B., and Johnson, K. H. (1990) Amino acid sequence from degu islet amyloid-derived insulin shows unique sequence characteristics. *Biochem Biophys Res Commun.* **169**, 571-577
82. Weiss, M. A. (2013) Diabetes mellitus due to the toxic misfolding of proinsulin variants. *FEBS Lett.* **587**, 1942-1950

[1]Abbreviations. αCT, α-chain C-terminal segment; CD, circular dichroism; CR, Cys-rich domain; DM, diabetes mellitus; FnIII-1, first fibronectin Type III domain; FnIII-2, second fibronectin Type III domain; FnIII-3, third fibronectin Type III domain; HPLC, high-performance liquid chromatography; HI, human insulin; IGF-I, II; insulin-like growth factors I and II; IGF-1R, Type I IGF receptor; IR, insulin receptor; IR-A and IR-B, A and B isoforms of the IR; KP, insulin *lispro*; L1, first Leu-rich repeat domain; L2, second Leu-rich repeat domain; ThT, thioflavin T; SEC, size-exclusion chromatography; TK, tyrosine kinase; UV, ultraviolet; WGA, wheat germ agglutinin and WT, wild type. Amino acids are designated by standard one- and three-letter codes.

[2]See Protein Databank entries 1TYL, 1TYM, 1G7A, 1EV3, 1ZNJ, 1EV6, 1BPH and 1DPH for further examples.

Figure Legends

Figure 1. Structure of insulin and the ectodomain of the IR. (*A*) Assembly of the zinc insulin coordinated WT hexamer. The insulin monomer (A- and B chains) forms zinc-free dimers *via* anti-parallel association of B-chain α-helices and C-terminal β-strands (brown); two zinc ions then mediate assembly of three dimers to form classical hexamer (T_6). The A chain is shown in *yellow* (ribbon representation), and the B chain in *light gray* (B1-B19) or *brown* (B20-B30). The conserved aromatic residues of Phe^{B24} and Phe^{B25} are shown as *black sticks* whereas Tyr^{B26} is *red*. (*B*) Inverted V-shaped assembly of IR ectodomain homodimer. One monomer is in ribbon representation (*labeled*), the second in surface representation. Domains are labeled as follows: L1, first Leu-rich repeat domain; CR, Cys-rich domain; L2, second Leu-rich repeat domain; FnIII-1,-2 and -3, first, second and third fibronectin Type III domains, respectively; and αCT: α-chain C-terminal segment. (*C*) Model of WT insulin in its receptor-free conformation overlaid onto the structure of the insulin-bound μIR (4). L1 and part of CR are shown in *powder blue*; αCT is shown in *purple*. Residues Phe^{B24}, Phe^{B25} and Tyr^{B26} are as in panel A. The B chain of μIR-bound insulin is shown in *black* (B6-B19); the *brown* tube indicates classical location within the overlay of residues B20-B30 of insulin in its receptor-free conformation, highlighting steric clash of B26-B30 with αCT. Coordinates were obtained from PDB entries 4INS, 3LOH, and 3W11.

Figure 2. Insulin sequence and μIR complex. (*A*) Sequence of WT insulin and sites of modification. A- and B chains are shown in *white* and *gray* respectively. Conserved aromatic residues Phe^{B24} and Phe^{B25} are highlighted as *black* circles. The present study focused on substitutions of Tyr^{B26} (*red* circle); additional substitutions were made at position B29 (Orn; *encircled* X) to facilitate semi-synthesis. (*B*) Stick representation of residues B20-B27 (carbon atoms (*green*), nitrogen atoms (*blue*) and oxygen atoms (*red*) packed between αCT and the L1-β_2 sheet. B-chain residues B8-B19 are shown as a *black* ribbon and the A chain as a *yellow* ribbon; residues A1-A3 are concealed behind the surface of αCT. Key contact surfaces of αCT with B24-B26 are highlighted in *magenta*, and of L1 with B24-B26 are highlighted in *cyan*; L1 and αCT surfaces not in interaction with B24-B26 are shown in lighter shades. Insertion of the B20-B27 segment between L1 and αCT is associated with a small rotation of the B20-B23 β-turn and changes in main-chain dihedral angles flanking Phe^{B24} (4). (*C*) Orthogonal view to (*B*), showing interaction of the side chain of Phe^{B24} with the nonpolar surface of the L1-β_2 sheet. Tyr^{B26} is hidden below the surface of αCT. Engagement of conserved residues A1-A3 against the nonpolar surface of αCT is shown at top. (*D*) Environment of Tyr^{B26} within Site 1 complex (stereo). Neighboring side chains in L1 and αCT are as labeled. Coordinates were obtained from PDB entry 4OGA.

Figure 3. Functional screening of insulin analogs. (*A*) Competitive receptor-binding assay of Orn^{B29}-insulin (*black squares*; line indicates fitted model); its K_d is estimated to be 0.042(±0.007) nM. Model curves simulated based on K_d values that are 10-fold (*red*) or 100-fold (*blue*) greater than that of Orn^{B29}-insulin are also shown. *Red* dots indicate binding of insulin analogs Leu^{B26}-Orn^{B29} (*top*), Met^{B26}-Orn^{B29} (*middle*), and Gln^{B26}-Orn^{B29} (*bottom*) at a concentration of 0.75 nM. Vertical axis: B/B_0 where B is ^{125}I-Tyr^{A14}-insulin bound by receptor at the designated insulin concentration and B_0 is ^{125}I-Tyr^{A14}-insulin bound by receptor in the absence of unlabeled insulin. (*B*) Coarse screening at analog concentration of 0.75 nM. The analogs were classified as being of low, intermediate, or high affinity depending on the degree of ^{125}I-Tyr^{A14}-insulin displacement.

Figure 4. HPLC size-exclusion chromatography and hormone self-assembly. (*A*) Retention times of the various analogs (1-5) are shown; identities are described in (*C*). Elution of ~ 50 % of Glu^{B26}-Orn^{B29} as a

large multimer of ~ 80 kDa is indicated by an asterisk (*5). (*B*) Plot of log molecular weight *versus* V_e/V_o of different molecular-mass standard proteins. V_e is elution volume of each protein and V_o, the column's void volume. Calibration: apoferritin (443 kDa, V_o), bovine serum albumin (67 kDa) ovalbumin (43 kDa), ribonuclease A (13.7 kDa), cytochrome C (12.4 kDa), and synthetic peptides (4 and 1.2 kDa). Line represents a linear fit whereas arrows indicate relative elution of analogs 1-5. (*C*) Masses of analogs determined from calibrated standards (fitted line). (*D-F*) HPLC SEC in presence of zinc and cyclohexanol. Proteins were fractionated as in (*A*) with inclusion of 50 mM cyclohexanol and 0.3 mM $ZnCl_2$; column was re-calibrated in this buffer. With one exception, the Orn^{B29}-insulin analogs, WT human insulin (HI) and insulin *lispro* (KP) each eluted as hexamers as indicated in (*E*) and (*F*). Although a small fraction of the Glu^{B26}-Orn^{B29}-insulin also eluted as a hexamer (5), most of the protein dissociated on the column with a broad elution profile (*5).

Figure 5. Visible absorption spectra of cobalt-stabilized hexamers and kinetics of metal-ion release. (*A*) Co^{2+} *d-d* bands of Orn^{B29}-insulin (*red*), Glu^{B26}-Orn^{B29}-insulin (*turquoise*), and Orn^{B26}-Orn^{B29} -insulin (*violet*) near 550 nm provide a signature of the R (or R_f) hexameric state. Amplitudes of both Orn^{B26} and Glu^{B26} variants are attenuated in relation to Orn^{B29}-insulin. Control spectra are provided by WT insulin (*black*) and KP-insulin (*gray*). Whereas attenuation of amplitude of the 550 nm band of the Orn^{B26} variant may be explained by the decreased hexamer formation of the analog, the marked differences in the Glu^{B26} spectrum may be the result of non-specific aggregates of the analog forming in aqueous solution, as suggested by gel filtration experiments. (*B*) Sequestration of cobalt ions from insulin analogs by EDTA: Orn^{B29}-insulin (*red*), Glu^{B26}-Orn^{B29} (*turquoise*) insulin, and Orn^{B26}-Orn^{B29} (*violet*) analogs are shown in relation to those of WT insulin (*black*) and KP-insulin (*gray*). Orn^{B26}-Orn^{B29}-insulin formed aggregates that precipitated from solution at intermediate stages of hexamer dissociation (marked by *black asterisk*): initial region of the curve was fitted to a monoexponential equation.

Figure 6. Studies of structure, stability and fibrillation. (*A*) Far-UV CD spectra of Orn^{B29}-insulin (*red*), Glu^{B26}-Orn^{B29}-insulin (*cyan*), Orn^{B26}-Orn^{B29}-insulin (*magenta*) and Ser^{B26}-Orn^{B29} insulin (*dark blue*) relative to WT insulin (open circles; *black*) at neutral pH 7.4 and 25 °C. Ellipticity was normalized per residue. (*B*) Corresponding guanidine-unfolding transitions as monitored at 222 nm. Thermodynamic stabilities were derived using a two-state model (see Table 2). Color code is as in *A*. (*C*) Histogram of ΔG_u values in kcal mol^{-1}. Marked changes in stability were evident depending on the identity of the substitution. (*D*) Dot plot of lag time (*days*) to fibril formation of insulin analogs. Onset of fibrillation was defined by a two-fold enhancement of ThT fluorescence; see main text for statistical analysis and *p* values.

Figure 7. Evolutionary constraints and insulin fibrillation. (*A*) Venn diagram showing intersection of multiple constraints: function, foldability, misfolding and assembly. We envisage that Tyr^{B26} is conserved due to its explicit roles in folding and assembly and implicit role in avoiding misfolding. (*B*) Surface representation of a T-state monomer (PDB entry 4INS) with residues B23-30 (stick model) within a groove between the A- and B chains. The aromatic side chains of Phe^{B24}, Phe^{B25} (both *dark gray*) and Tyr^{B26} (*red*) are shown. (*C*) General scheme of insulin fibrillation *via* a partially unfolded monomer intermediate. The native state is protected by classic self-assembly. Disassembly leads to an equilibrium between native and partially folded monomers. The receptor-bound conformation of insulin (*top*) may also participate in this equilibrium. This partial fold may unfold completely (*bottom*) as an off-pathway event or aggregate to form a nucleus en route to a proto-filament (*right*).

Table 1. Receptor-Binding Affinities of Insulin Analogs[a]

B26 residue	K_d (nM)	B26 residue	K_d (nM)
Tyr[b]	0.042 ± 0.007	Pro	I[d]
Gly	H[c]	Ser	0.021 ± 0.003
Ala	0.042 ± 0.007	Thr	I
Val	0.12 ± 0.02	Cys	ND[e]
Leu	1.2 ± 0.2	Asn	H
Ile	0.52 ± 0.08	Asp	H
Met	I	Gln	0.043 ± 0.007
Glu	0.021 ± 0.002	His	H
Phe	0.10 ± 0.020	Lys/Arg	ND[f]
Trp	H	Orn[g]	0.038 ± 0.006

[a]Analogs were prepared in a template in which Lys^{B29} was substituted by Orn unless otherwise noted. Assays employed the B isoform of the purified and detergent-solubilized IR as described in the Experimental Procedures.

[b]This represents Orn^{B29}-insulin; the dissociation constant of WT insulin under these conditions was 0.042 nM.

[c]H represents the high-affinity group in the initial coarse screening (Fig. 3*B*).

[d]I represents the intermediate-affinity group in the initial coarse screening (Fig. 3*B*).

[e]ND, not determined as the Cys^{B26} analog was not prepared.

[f]ND, not determined as substitution of Tyr^{B26} by Lys or Arg would have complicated semi-synthesis (see Experimental Procedures).

[g]Orn^{B26} provided a model of a basic side chain.

Table 2. Properties of Insulin Analogs

analog	ΔG_u[a] (kcal mol^{-1})	C_{mid} (M)	m (kcal mol^{-1} M^{-1})	fibrillation lag time[b] (days (N))
wild-type insulin	3.4 ± 0.1	4.8 ± 0.1	0.69 ± 0.02	4.4 ± 4.9 (15)
Orn^{B29}-insulin	3.2 ± 0.1	4.8 ± 0.1	0.66 ± 0.01	13.1 ± 6.5 (14)
Glu^{B26}-Orn^{B29}	2.3 ± 0.1	4.4 ± 0.1	0.53 ± 0.02	2.7 ± 0.6 (3)
Orn^{B26}-Orn^{B29}	2.5 ± 0.1	4.3 ± 0.2	0.59 ± 0.03	2.0 ± 0.1[c] (3)
Ser^{B26}-Orn^{B29}	2.3 ± 0.1	4.3 ± 0.3	0.53 ± 0.04	2.0 ± 0.1[c] (3)

[a]Thermodynamic parameters were inferred from CD-detected guanidine denaturation data by application of a two-state model.

[b]Fibrillation lag times pertain to zinc-free wild-type insulin (in a monomer-dimer equilibrium) and analogs (monomeric); each protein was made 60 μM in phosphate-buffered saline (pH 7.4). A twofold increase over baseline in ThT fluorescence provided a criterion for onset of fibrillation.

[c]All individual samples in this set exhibited the same lag time of 2 days. As the method employed in this study could not distinguish fibril lag times with a resolution given in hours, some variance was added to the data by adding ± 0.1 to individual data points in order to obtain standard deviations.

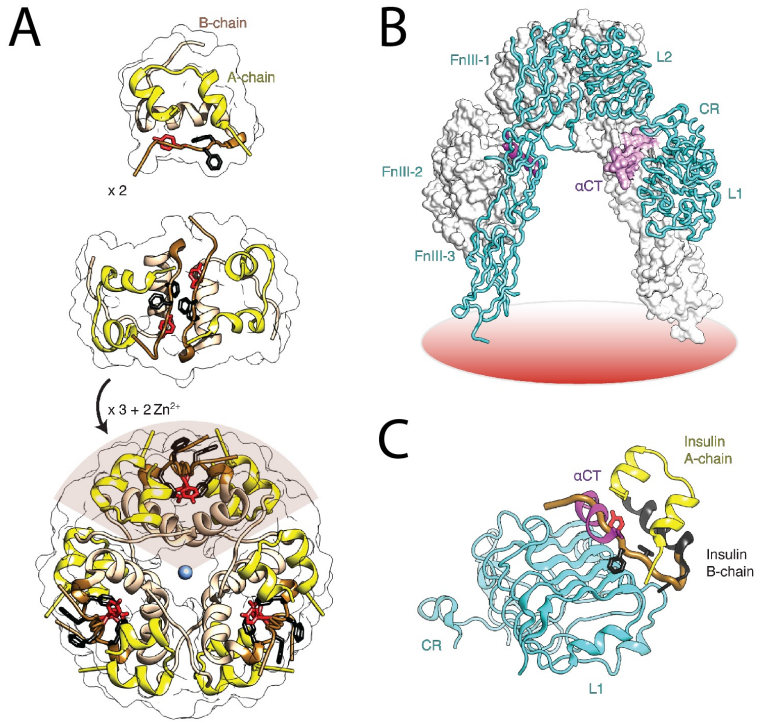

Figure 1

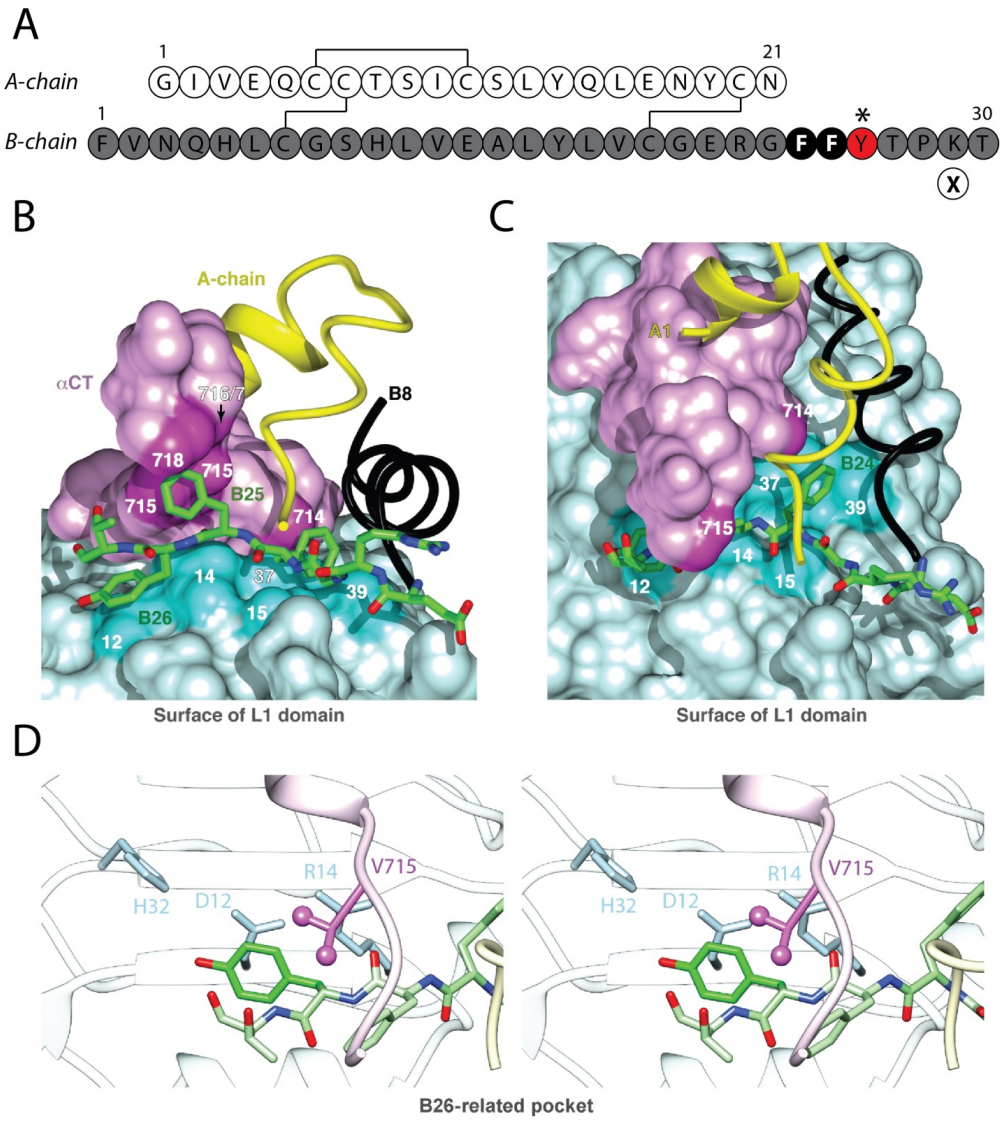

Figure 2

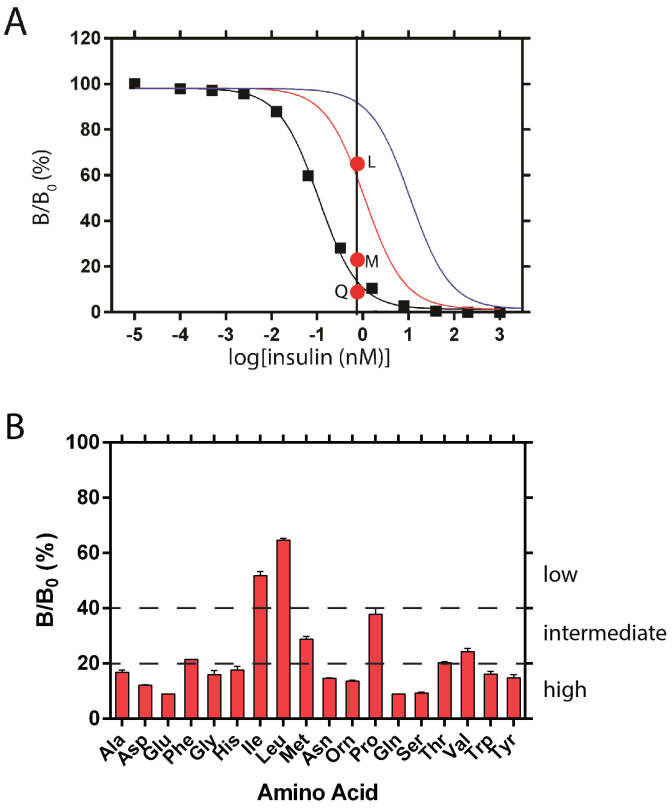

Figure 3

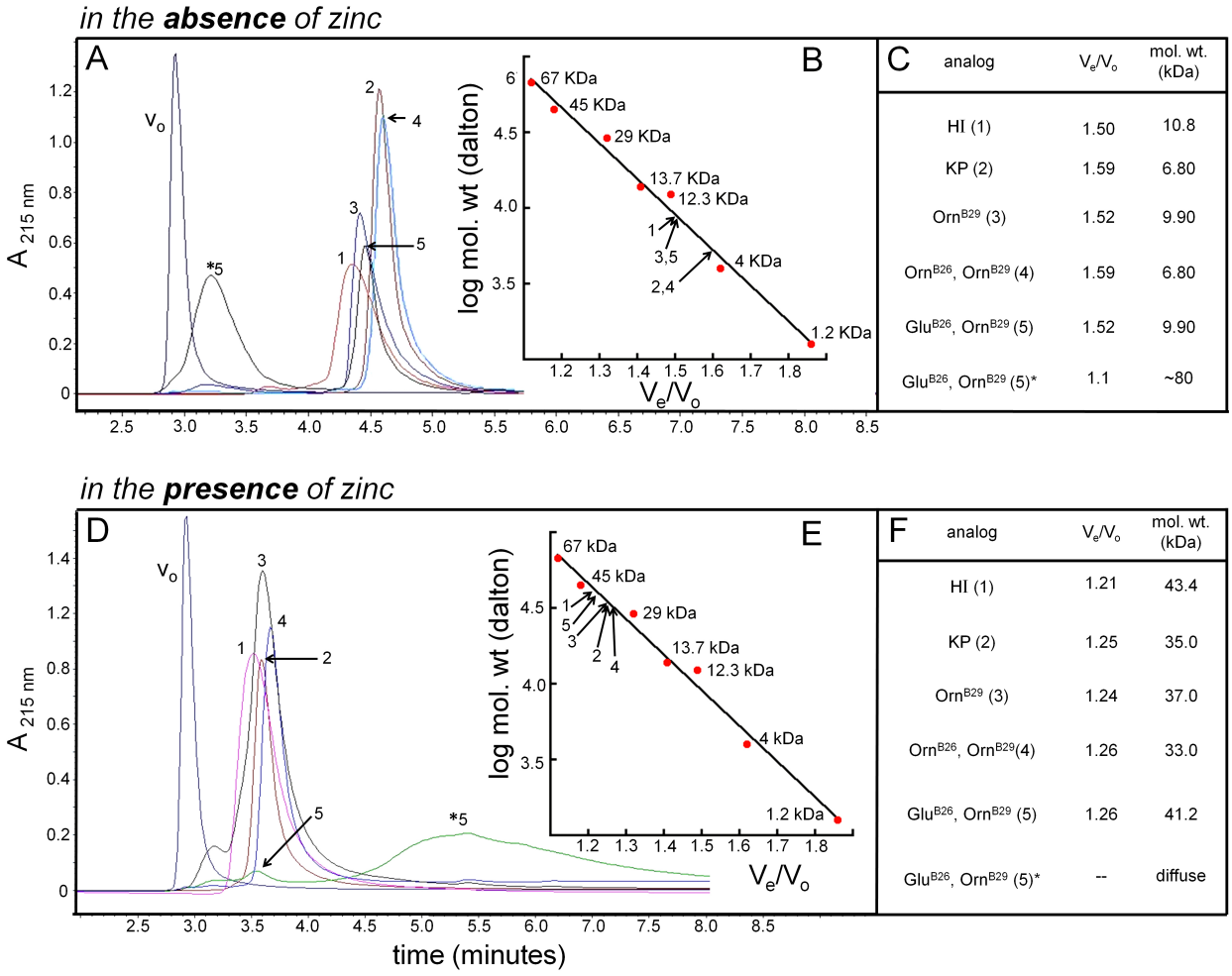

Figure 4

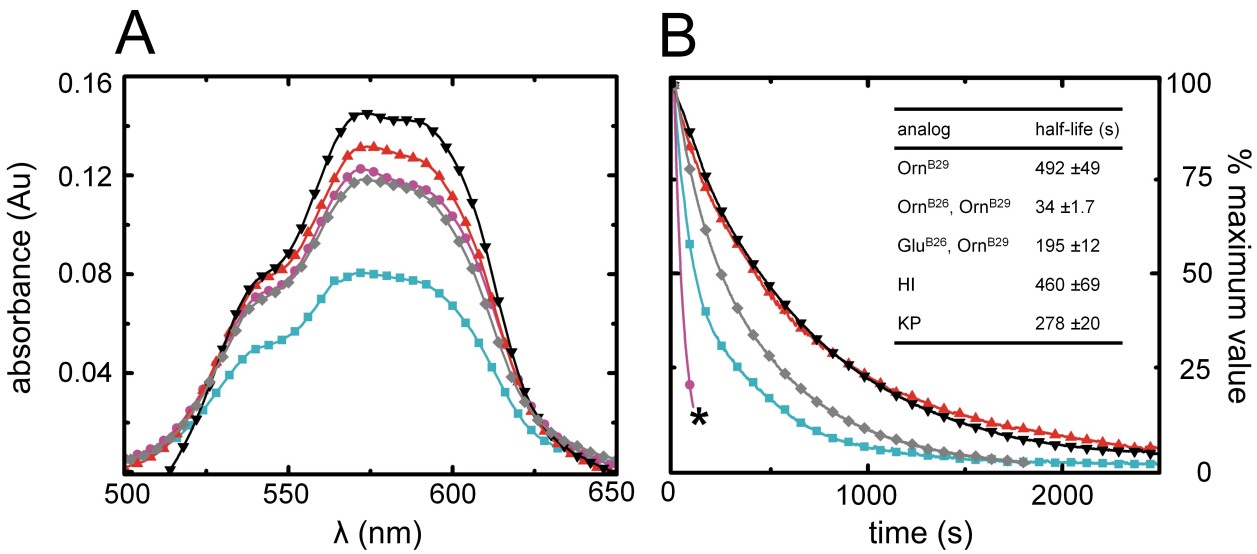

Figure 5

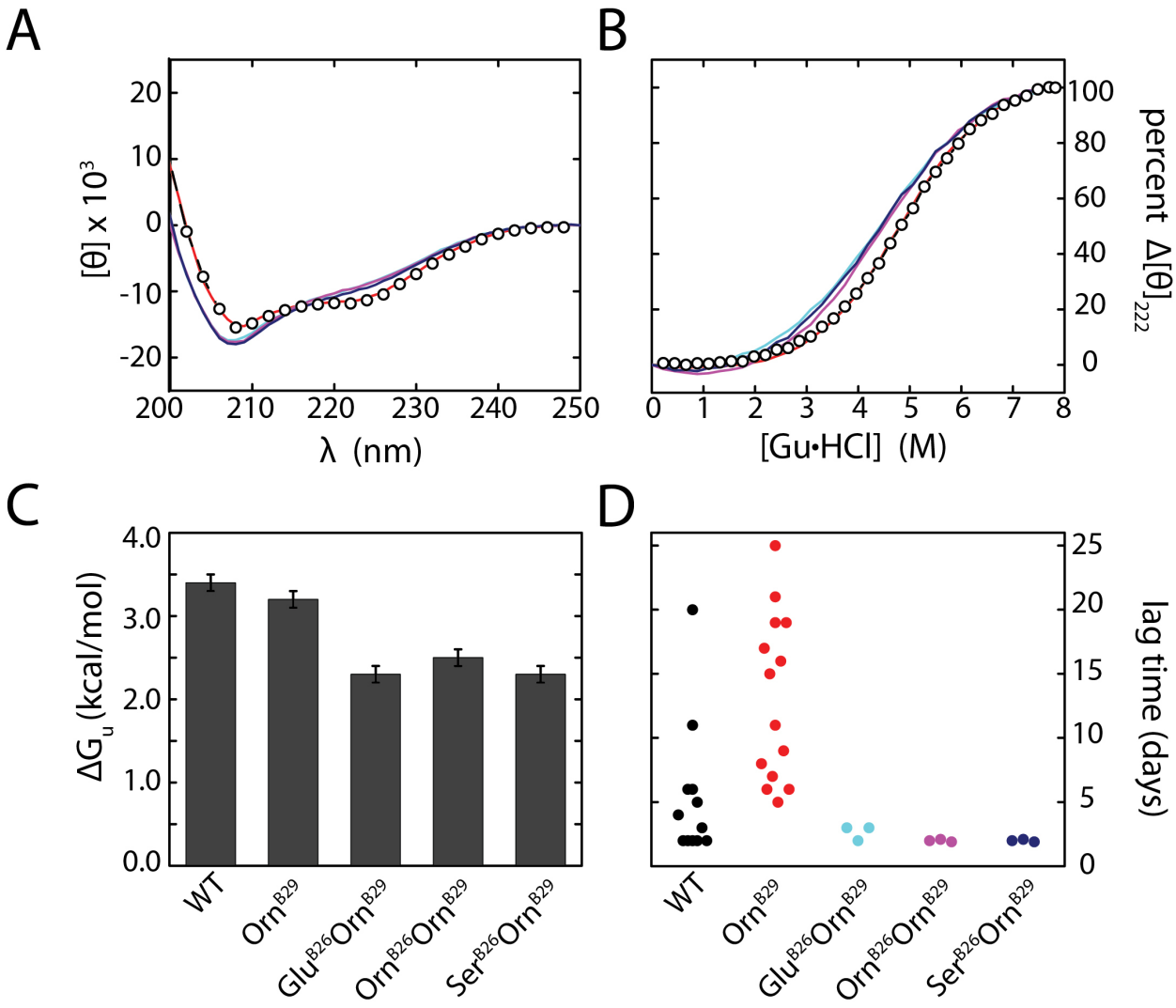

Figure 6

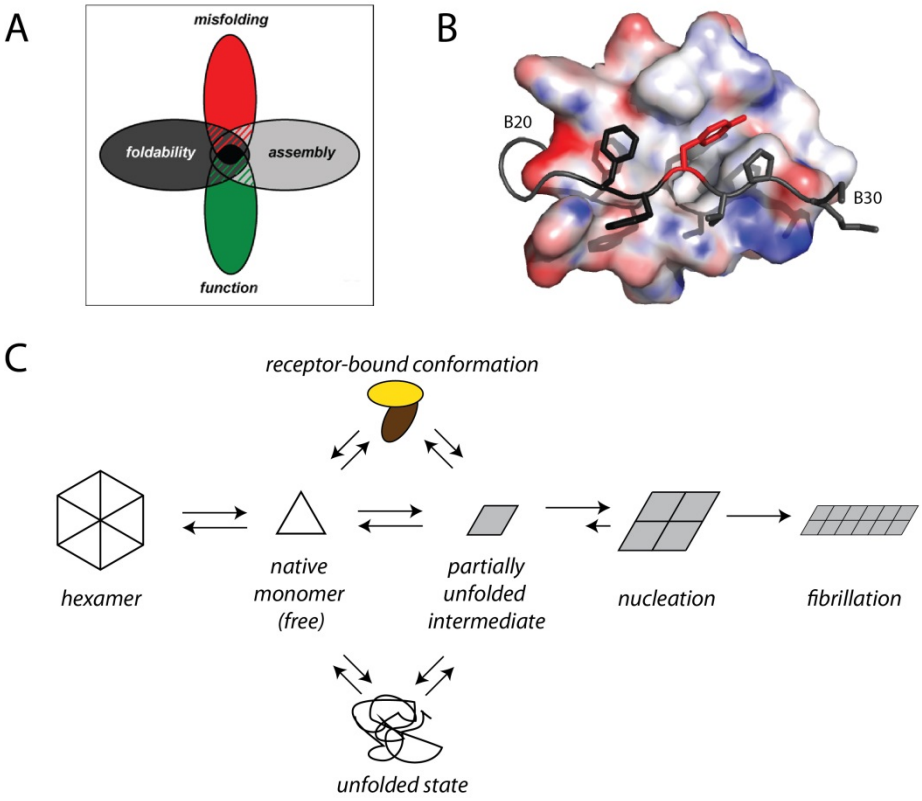

Figure 7

Contribution of Tyr^{B26} to the Function and Stability of Insulin. Structure-activity relationships at a conserved hormone-receptor interface

Vijay Pandyarajan, Nelson B. Phillips, Nischay K. Rege, Michael C. Lawrence, Jonathan Whittaker and Michael A. Weiss

J. Biol. Chem. published online April 26, 2016
